A Joint Azimuth Multichannel Cancellation (JAMC) Antibarrage Jamming Scheme for Spaceborne SAR

Shuohan Cheng, Xilong Sun, Yonghua Cai, Huifang Zheng, Weidong Yu, *Member, IEEE*, Yanyan Zhang, *Member, IEEE*, and Sheng Chang

***Abstract*—The azimuth multichannel synthetic aperture radar (SAR) increases the swath width by reducing the pulse repetition frequency (PRF), thus providing an effective scheme for realizing high-resolution and wide-swath (HRWS) imaging simultaneously. However, the quality of multichannel SAR images will suffer from electromagnetic jamming in the electronic antagonism environment. The existing channel cancellation methods not only require high positioning accuracy of the jammer and high PRF of the SAR system, but also remain periodic dark stripes, which reduce the readability of the SAR images. To solve these problems, this article proposes a scheme for multichannel SAR to locate the barrage jammer and suppress jamming signals. First, by establishing the least L^1-norm optimization model on the echoes after channel cancellation, the location of the jammer in both azimuth and range directions can be accurately estimated. Then, based on the estimated jammer position, a joint cancellation filter is constructed to remove the jamming signal from the contaminated multichannel SAR data. And the reconstruction filter is designed according to the characteristics of the remaining signal, so that the SAR system reduces the requirement for high PRF. Finally, for the case of dark strips, this article calculates the image amplitude equalization coefficient by deducing the azimuth modulation function, and a uniform HRWS SAR image without jamming is acquired. Results of simulated and measured data validate that the proposed method can effectively remove jamming signals and obtain the HRWS SAR images.**

***Index Terms*—Azimuth compensation, jammer localization, jamming signal suppression, least L^1-norm, multichannel synthetic aperture radar (SAR).**

Manuscript received 30 July 2022; revised 23 September 2022; accepted 30 October 2022. Date of publication 11 November 2022; date of current version 23 November 2022. This work was supported by the Reserve Talents Project of National High-level Personnel of Special Support Program under Grant Y9G0100BF0. *(Corresponding author: Huifang Zheng.)*

Shuohan Cheng, Weidong Yu, Yanyan Zhang, and Sheng Chang are with the Department of Space Microwave Remote Sensing System, Aerospace Information Research Institute, Chinese Academy of Sciences, Beijing 100190, China, and also with the School of Electronic, Electrical and Communication Engineering, University of Chinese Academy of Sciences, Beijing 100049, China (e-mail: chengshuohan19@mails.ucas.ac.cn; ywd@mail.ie.ac.cn; caszyymail@163.com; changsheng19@mails.ucas.ac.cn).

Xilong Sun is with the Beijing Remote Sensing Information Institute, Beijing 100192, China (e-mail: 396576571@qq.com).

Yonghua Cai is with the National Key Laboratory of Microwave Imaging Technology, Aerospace Information Research Institute, Chinese Academy of Sciences, Beijing 100190, China, and also with the School of Electronic, Electrical and Communication Engineering, University of Chinese Academy of Sciences, Beijing 100049, China (e-mail: caiyonghua19@mails.ucas.edu.cn).

Huifang Zheng is with the Department of Space Microwave Remote Sensing System, Aerospace Information Research Institute, Chinese Academy of Sciences, Beijing 100190, China (e-mail: bluebird_855@126.com).

Digital Object Identifier 10.1109/JSTARS.2022.3221402

I. Introduction

As ITS all-day and all-weather capabilities to conduct remote sensing/surveillance, synthetic aperture radar (SAR) plays an increasingly important role both in civil exploration and military application [1], [2], [3], [4], [5], [6]. In order to meet the requirements of frequent observation in large-scale areas, an azimuth multichannel SAR system is developed to provide the high-resolution and wide-swath (HRWS) image simultaneously [7], [8], [9]. The system alleviates the inherent contradiction between the high pulse repetition frequency (PRF) and swath width, and has been widely used in ground moving target indication, sea clutter suppression, etc. [10], [11], [12]. However, with the rapid development of microwave technology and the proliferation of radio frequency equipment, SAR is highly likely to be interfered by various active electronic devices in a complex electromagnetic environment [13]. Therefore, it is crucial to develop effective jamming suppression methods to recover the contaminated azimuth multichannel SAR data.

Generally, SAR jamming can be divided into two types: deception jamming and barrage jamming, and this article mainly focuses on barrage jamming. For deception jamming, the jammer usually modulates and transmits the intercepted SAR signal, which eventually forms false targets in the focused image to confuse opponents. Unlike deception jamming, the barrage jammer usually emits noise-like and high-power jamming to cover the desired signal, so that the required information of the imaging area is submerged in the jamming signal [14], [15], [16], [17]. Compared with deception jamming, the principle of barrage jamming is simple and easy to be implemented. The jammer only needs to acquire the frequency range of the SAR signal, and the high-power jamming signal emitted can effectively cover the SAR echo [14].

In the field of jamming suppression technology research, the corresponding antijamming algorithms of multichannel SAR, including the jammer localization methods and the jamming suppression methods, have also received certain attention in the recent years. For the localization of the jammer, Yu et al. [18] proposed a single RFI localization algorithm based on the conjugate cross-correlation of dual-channel SAR signals, which strictly requires that the energy of the interference signal is much stronger than real target signal. Moreover, the sensitivity of iterative initial value also seriously affects the localization accuracy. Lin et al. [19] used the direction of arrival (DOA) method to obtain the angles between the SAR and the jammer

at different azimuth times, and then, the azimuth coordinate of the jammer in the scene could be acquired. However, the DOA method is mainly designed for array antennas, and the distance between adjacent array elements is required to be no greater than half of the wavelength. Obviously, the channel phase center distance cannot meet this condition in any multichannel SAR system. When applying the DOA method, a series of fuzzy angles are generated, which are difficult to be distinguished from the real estimated angle.

For the jamming suppression algorithm of multichannel SAR, the space time adaptive processing jamming suppression technology in the slow time domain and the fast time domain has been proposed in [20] and [21], which takes the spatial sampling information provided by multichannel and the correlation pulse sequence obtained in synthetic aperture time to design space-time adaptation filter, so as to suppress the active jamming. Inspired by the displaced phase center antenna clutter suppression technology [22], a dual-channel cancellation method is presented in [19] and [23] to suppress the jamming signal. The dual-channel cancellation method utilizes the phase relationship between the echo signals received by different channels to eliminate the signal from the fixed-point jammer. This method is easy to be implemented and has low computational complexity. But periodic dark stripes will be formed in the imaging result, which weaken the readability of the image. In order to alleviate this issue, Ma et al. [24] proposed a three-channel cancellation method with unequal channel spacing, which effectively extends the period of dark strips and improves the imaging quality. However, the above jamming suppression methods all require that the signals have unambiguous spectrum to ensure the echo of a single channel can be imaged, resulting in the loss of the HRWS capability of multichannel SAR directly.

To ensure the azimuth multichannel SAR can work normally in the low PRF mode while suppressing the jamming, we propose a joint azimuth multichannel cancellation (JAMC) antibarrage jamming scheme, including the jammer localization and joint channel cancellation technology. First, the multichannel SAR echo signal model in a single-jammer environment is constructed. Second, the least L^1-norm optimization model of echo signal is established by using the principle of dual-channel cancellation method, and the position of jammer in the scene is obtained with high accuracy. Then, the multichannel signals are jointly canceled and reconstructed according to the estimated position of the jammer. At the cost of only losing one channel degree of freedom, the jamming suppression is successfully achieved and the HRWS capability of multichannel SAR systems is retained simultaneously. Finally, the azimuth modulation of the SAR image brought by the joint cancellation is deduced and compensated, and the uniform HRWS SAR image after jamming suppression is obtained.

The contribution of this article can be summarized as follows.

1) Establish a least L^1-norm optimization model of the echoes after channel cancellation, and the location of the jammer in both azimuth and range directions can be accurately estimated by an iterative method. According to the estimated coordinate of the jammer, a joint-channel-cancellation filter is constructed to remove the jamming signals at the same time.

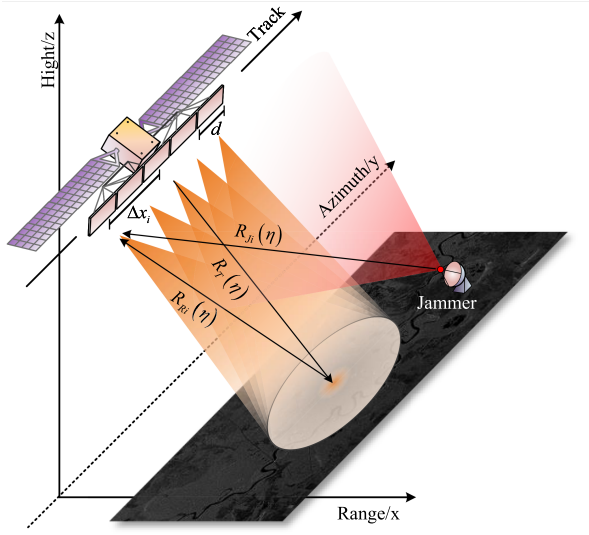

Fig. 1. Imaging geometric configuration of the multichannel SAR.

2) According to the signal characteristics after channel cancellation, the reconstruction filter is designed to complete the signal reconstruction, so as to achieve unambiguous imaging in the low PRF mode. For the case of dark strips, this article calculates the azimuth modulation brought by the cancellation process to the real signal, and the image amplitude equalization coefficient is obtained. Based on this, the image is weighted and the HRWS SAR image is obtained.

The rest of this article is organized as follows. In Section II, the multichannel echo model in the environment with a single jammer is given, and the principle of channel cancellation is briefly introduced. In Section III, the JAMC barrage jamming suppression scheme is presented in detail. In Section IV, simulations and real data experiments are presented to demonstrate the effectiveness of the proposed method. Finally, Section V concludes this article.

II. Signal Model and Cancellation Principle

A. Signal Model

For an azimuth multichannel SAR system, the signal is transmitted by a single channel and received by all the subapertures. Fig. 1 shows the geometric configuration of the multichannel SAR in a single-jammer environment. A Cartesian coordinate system is established with the subsatellite point when the azimuth time $\eta = 0$ as the origin. The x-axis points to the normal direction of the multichannel antenna, y-axis and z-axis represent the moving direction of the radar platform and the direction away from the center of the earth, respectively. Taking the middle channel of the antenna as the transmitting channel, $R_T(\eta)$ and $R_{Ri}(\eta)$, which represent the distance from the transmitting channel to the target and the distance from the target to the ith receiving channel, respectively, can be expressed as

$$R_T(\eta) = \sqrt{R_0^2 + (V_r\eta)^2} \tag{1}$$

$$R_{Ri}(\eta) = \sqrt{R_0^2 + (V_r\eta - \Delta x_i)^2} \tag{2}$$

where $i = 1, 2, \ldots, I$. I is the number of channels. V_r is the platform velocity, and R_0 signifies the nearest slant range from the transmitting channel to the ground targets. $\Delta x_i = (i_{\text{ref}} - i)d$ denotes the distance between the i_{ref}th channel and the ith channel. i_{ref} signifies the reference channel. d denotes the channel spacing. The echo signal is transmitted by the reference channel i_{ref} and received by the channel i, so the instantaneous slant range of the signal received by the ith channel can be obtained as

$$R_i(\eta) = \frac{R_T(\eta) + R_{Ri}(\eta)}{2}. \tag{3}$$

Suppose the coordinate of the jammer is $(x_J, y_J, 0)$. The jamming signal continuously generated and transmitted by the jammer is directly received by the channels through one-way propagation. Therefore, the distance from the jammer to the ith receiver channel can be expressed as

$$R_{Ji}(\eta) = \sqrt{R_J^2 + (V_r\eta - y_J - \Delta x_i)^2} \tag{4}$$

where $R_J = \sqrt{x_J^2 + H^2}$ signifies the nearest slant range between jammer and the transmitting channel. H is the height of the platform.

According to (3) and (4), the target signal and the jamming signal received by the ith channel can be, respectively, formulated as

$$\begin{aligned} s_{Ti}(\tau,\eta) = {} & \omega_r\left\{\tau - \frac{2R_i(\eta)}{c}\right\}\omega_a\{\eta - \eta_c\} \\ & \times \exp\left\{-j4\pi f_0\frac{R_i(\eta)}{c}\right\} \\ & \times \exp\left\{j\pi K_r\left(\tau - \frac{2R_i(\eta)}{c}\right)^2\right\} \end{aligned} \tag{5}$$

$$s_{Ji}(\tau,\eta) = \omega_J\left(\tau - \frac{R_{Ji}(\eta)}{c}\right)\exp\left\{j2\pi f_0\left(\tau - \frac{R_{Ji}(\eta)}{c}\right)\right\} \tag{6}$$

where τ signifies the range fast time, η_c signifies the azimuth center time, c signifies the speed of light, f_0 is the carrier frequency, K_r is the chirp rate, ω_r and ω_a are the range envelope and the azimuth envelope, respectively, ω_J represents the signal form of barrage jamming, such as the radio frequency noise interference, the narrowband interference, and the wideband interference [25]. Here, we adopt a general model for the jamming signal, which is expressed as

$$\begin{aligned} w_J\left(\tau - \frac{R_{Ji}(\eta)}{c}\right) = {} & U_n\left(\tau - \frac{R_{Ji}(\eta)}{c}\right) \\ & \times \exp\left\{j\pi k_r\left(\tau - \frac{R_{Ji}(\eta)}{c}\right)^2 + j\varphi_1\right\} \end{aligned} \tag{7}$$

where $U_n(\tau)$ is the Gaussian noise, k_r denotes the chirp rate of the jamming signal, and φ_1 is the phase of the jamming signal, and obeys a uniform distribution of $[0, 2\pi]$.

Thus, the signal received by the ith channel can be described as

$$s_i(\tau,\eta) = s_{Ti}(\tau,\eta) + s_{Ji}(\tau,\eta) + n_i(\tau,\eta) \tag{8}$$

where n_i denotes the receiver noise. The SAR echo signal $s_{Ti}(\tau,\eta)$ undergoes two-way slant range attenuation, while the jamming signal $s_{Ji}(\tau,\eta)$ transmitted by the jammer to the SAR only experiences one-way attenuation, which means that the jamming signal $s_{Ji}(\tau,\eta)$ has an absolute advantage in power compared with the SAR echo signal $s_{Ti}(\tau,\eta)$ [26].

B. Channel Cancellation Principle

The channel cancellation method mainly utilizes the phase differences of the jamming signals received by different channels to suppress the jamming signal. The signal needs to be multiplied by a phase compensation factor, so that the phase of the jamming signals in different receiving channels to be canceled is the same.

Assuming that the ith channel signal is canceled with the jth one, the phase compensation factor for the ith channel signal is

$$g_{ij}(\eta) = \exp\left\{-j2\pi\frac{R_{Jj}(\eta) - R_{Ji}(\eta)}{\lambda}\right\} \tag{9}$$

where λ is the wavelength. Then, the cancellation result is expressed as

$$\begin{aligned} s_{ij}(\tau,\eta) &= g_{ij}(\eta)s_i(\tau,\eta) - s_j(\tau,\eta) \\ &= s_{Tij}(\tau,\eta) + s_{Jij}(\tau,\eta) + n_{ij}(\tau,\eta). \end{aligned} \tag{10}$$

The first term $s_{Tij}(\tau,\eta)$ of (10) denotes the cancellation result of useful echo, which can be expressed as

$$s_{Tij}(\tau,\eta) = g_{ij}s_{Ti}(\tau,\eta) - s_{Tj}(\tau,\eta). \tag{11}$$

The second term $s_{Jij}(\tau,\eta)$ is the jamming signal cancellation result and can be expressed as

$$\begin{aligned} s_{Jij}(\tau,\eta) &= g_{ij}(\eta)\, s_{Ji}(\tau,\eta) - s_{Jj}(\tau,\eta) \\ &= \left[\omega_J\left(\tau - \frac{R_{Ji}(\eta)}{c}\right) - \omega_J\left(\tau - \frac{R_{Jj}(\eta)}{c}\right)\right] \\ &\quad \times \exp\left\{j2\pi f_0\left(\tau - \frac{R_{Jj}(\eta)}{c}\right)\right\}. \end{aligned} \tag{12}$$

It is worth noting that the difference between $R_{Ji}(\eta)$ and $R_{Jj}(\eta)$ is in centimeters, and $(R_{Ji}(\eta) - R_{Jj}(\eta))/c$ is in the order of e^{-10}, which is much smaller than $1/F_r$ (a range gate time). Therefore, it can be considered that the jamming signal envelopes of different channels are located in the same distance unit, and we can get

$$s_{Jij}(\tau,\eta) \approx 0. \tag{13}$$

Then, (10) can be rewritten as

$$s_{ij}(\tau,\eta) \approx s_{Tij}(\tau,\eta) + n_{ij}(\tau,\eta). \tag{14}$$

It can be seen that the jamming signal in $s_{ij}(\tau,\eta)$ is eliminated after the above cancellation processing, and only the target signal $s_{Tij}(\tau,\eta)$ and noise $n_{ij}(\tau,\eta)$ are reserved. Then, well-focused SAR imaging result can be obtained by the conventional imaging algorithms.

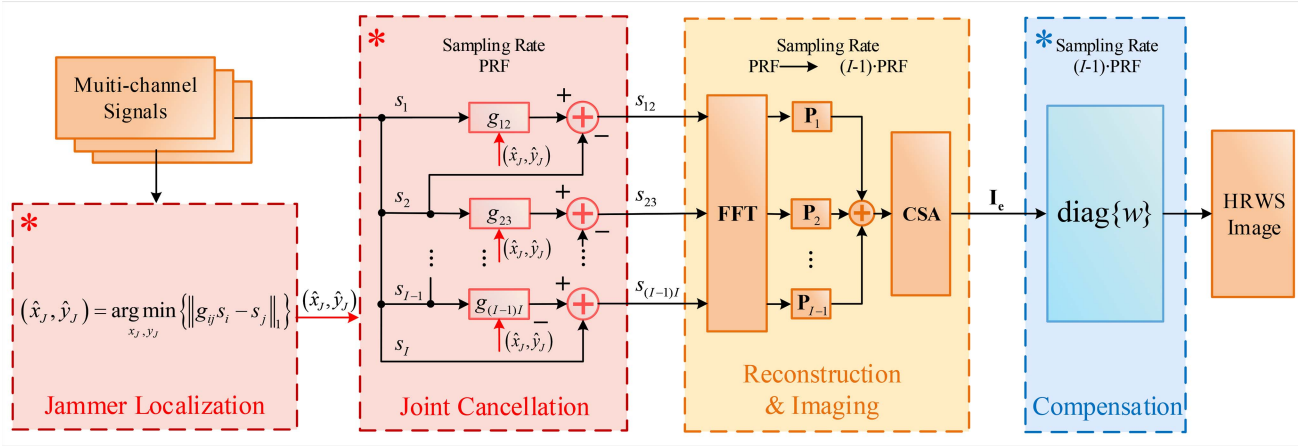

Fig. 2. Flowchart of the proposed scheme. (* Our novelty).

III. JAMC Scheme

In this section, the proposed multichannel SAR barrage jamming suppression scheme is introduced in detail. The framework of the proposed scheme is shown in Fig. 2. The main steps include the localization of jammer, joint cancellation of multichannel signals, signal reconstruction after jamming removal, and azimuth compensation in the focused image domain. After this, a uniform HRWS image can be obtained.

A. Localization of the Jammer

It is not difficult to find that the phase compensation factor in (9) is a function of the location of the jammer $(x_J, y_J, 0)$, which can be re-expressed as $g_{ij}(\eta, x_J, y_J)$. In other words, the premise of realizing channel cancellation is that the location of the jammer $(x_J, y_J, 0)$ is known, so that the phase compensation factor can be constructed according to the instantaneous slant range. Therefore, the location of the jammer plays a crucial role in this jamming suppression method, and the accuracy of the jammer location directly affects the performance of the jamming suppression.

For the multichannel SAR in a single-jammer environment, the instantaneous jamming signal will be received by the SAR receiver, which greatly raise the amplitude of the whole received signal. According to (9), when the location of the jammer is known, the phase compensation factor $g_{ij}(\eta, x_J, y_J)$ is also determined. The jamming signal will be removed after the channel cancellation process, which means that the amplitude of the signal $s_{ij}(\tau, \eta)$ will reach the minimum value. Therefore, the localization of the jammer can be transformed into finding a coordinate $(\hat{x}_J, \hat{y}_J)$, and constructing the phase compensation factor $g_{ij}(\eta, \hat{x}_J, \hat{y}_J)$ to minimize the L^1-norm of the signal after cancellation, then the coordinate can be considered as the jammer's location. Thus, the least L^1-norm optimization model to locate the jammer is established as

$$(\hat{x}_J, \hat{y}_J) = \underset{\hat{x}_J, \hat{y}_J}{\arg\min} \left\{ \left\| g_{ij}(\eta, \hat{x}_J, \hat{y}_J)\, s_i(\tau, \eta) - s_j(\tau, \eta) \right\|_1 \right\}$$
$$\text{s.t. } |\hat{x}_J| \le x_{\max}, |\hat{y}_J| \le y_{\max} \tag{15}$$

where $\|\cdot\|_1$ represents the L^1-norm of the matrix, that is, the sum of the absolute values of the elements of the matrix. $x_{\max}$ and $y_{\max}$, respectively, represent the upper limit of the range location and azimuth location of the jammer in the scene. There is no analytical solution for the minimum L^1-norm model, so the iterative method is used to acquire the numerical solution. Even so, the optimization problem is not a difficult numerical optimization problem. There are many mature algorithms, such as interior point method [27], [28] and sequential quadratic programming [29], that can be used to solve the problem in (15), and have good performance both in speed and accuracy.

The distance term $R_{Ji}(\eta)$ and $R_{Jj}(\eta)$ in (9) can be expanded by Taylor series and retained to the quadratic term, which can be expressed as

$$g_{ij}(\eta, x_J, y_J) \approx \exp\left\{ -j2\pi \frac{\left[V_r\eta - y_J - \Delta x_j - \frac{1}{2}(j-i)\,d\right](j-i)\,d}{\lambda\sqrt{x_J^2 + H^2}} \right\}. \tag{16}$$

According to the periodicity of the trigonometric function, $g_{ij}(\eta, x_J, y_J)$ is the periodic function of y_J, which means that the actual jammer location may be

$$y_J = \hat{y}_J + k \cdot \frac{\lambda\sqrt{x_J^2 + H^2}}{(j-i)\,d} \tag{17}$$

where $k = 0, \pm1, \pm2, \ldots$, represents the kth ambiguity location of the jammer, so the azimuth position of the jammer has a series of ambiguous solutions with $\frac{\lambda\sqrt{x_J^2+H^2}}{(j-i)d}$ as the period. Usually, the signals of two adjacent channels are selected to establish the optimization model, that is, $j - i = 1$. In this case, the ambiguity period is at the maximum value, and the obtained ambiguity number of the jammer azimuth locations in the scene is the least. Moreover, the ambiguity of azimuth location has no effect on channel cancellation processing. No matter which possible azimuth location of the jammer is obtained, the phase compensation factor $g_{ij}(\eta, x_J, y_J)$ is the same, and the jamming

signal can still be accurately removed during channel cancellation processing.

In practice, there are inevitable channel errors such as amplitude error and phase error between channels, which will affect the accuracy of the proposed localization method. In general, for multichannel SAR systems, the amplitude error is small and easy to correct, so the effect on the proposed method can be ignored. Therefore, we only need to account for the phase error.

According to (10), for adjacent channels with channel phase error, there are

$$\begin{aligned} s_{i.i+1}(\tau,\eta) &= s_i(\tau,\eta)g_{i,i+1}(\eta)\exp(j\Delta\varphi) - s_{i+1}(\tau,\eta) \\ &= s_e(\tau,\eta)\exp\left\{j\frac{2\pi d}{\lambda R_J}\cdot(y_J+\Delta y)\right\} - s_{i+1}(\tau,\eta) \end{aligned} \tag{18}$$

with

$$\begin{aligned} s_e(\tau,\eta) &= s_i(\tau,\eta) \\ &\quad\times\exp\left\{-j\frac{2\pi}{\lambda}\cdot\frac{(V_r\eta-(2i_{\mathrm{ref}}-2i+1)d)\cdot d}{R_J}\right\} \end{aligned} \tag{19}$$

$$\Delta y = \frac{\lambda R_J}{2\pi d}\cdot\Delta\varphi. \tag{20}$$

From (18), we can find that the phase error will only affect the estimation of the azimuth coordinates and has little effect on the range coordinates. When the channel phase error is $\Delta\varphi$, the azimuth estimated coordinate value of the jammer is deviated by Δy.

After the channel error calibration [30], [31], [32], the value of the residual phase error between the channels is already very small. For multichannel SAR systems, since the localization processing can be completed by only two channels, we can use different adjacent channels to estimate the location for multiple times and obtain the mean value, so as to improve the localization accuracy and reduce the influence of channel errors.

B. Multichannel Joint Cancellation Processing

The traditional channel cancellation method theoretically only needs two channel signals, and the PRF needs to satisfy the Nyquist sampling law so that the signal after channel cancellation can be imaged without azimuth ambiguity. However, for a multichannel SAR system with more than two channels, channel redundancy will be caused. To make matters worse, an excessively high PRF would both burden the system and make wide-swath imaging impossible. This is obviously contrary to the original intention of HRWS imaging of multichannel SAR systems.

To make full use of multichannel signals, a multichannel joint cancellation method is proposed to achieve HRWS imaging while suppressing jamming signals. Considering the signals of all channels, (8) is reformulated by a joint signal matrix as

$$\mathbf{s} = \left[s_1(\tau,\eta),\ldots,s_i(\tau,\eta),\ldots,s_I(\tau,\eta)\right]^T \tag{21}$$

where the superscript $\{\cdot\}^T$ signifies the transpose operation. According to the estimated jammer location, the joint cancellation filter is constructed as

$$\mathbf{G}(\eta) = \begin{bmatrix} g_{12}(\eta) & -1 & 0 & \cdots & 0 \\ 0 & g_{23}(\eta) & -1 & \ddots & \vdots \\ \vdots & \ddots & \ddots & \ddots & 0 \\ 0 & \cdots & 0 & g_{(I-1)I}(\eta) & -1 \end{bmatrix} \tag{22}$$

where $g_{(i-1)i}(\eta)$is the phase compensation factor in (9). The remaining signal filtered by (22) is jamming free, which can be expressed as

$$\begin{aligned} \mathbf{s}_1(\tau,\eta) &= \mathbf{G}(\eta)\,\mathbf{s}(\tau,\eta) \\ &= \left[s_{12}(\tau,\eta),\ldots,s_{(i-1)i}(\tau,\eta),\ldots s_{(I-1)I}(\tau,\eta)\right]^T \end{aligned} \tag{23}$$

where

$$\begin{aligned} s_{(i-1)i}(\tau,\eta) &= g_{(i-1)i}(\eta)\,s_{i-1}(\tau,\eta) - s_i(\tau,\eta) \\ &\approx g_{(i-1)i}(\eta)\,u_{i-1}(\tau,\eta)\exp\left\{-j4\pi\frac{R_{i-1}(\eta)}{\lambda}\right\} \\ &\quad - u_i(\tau,\eta)\exp\left\{-j4\pi\frac{R_i(\eta)}{\lambda}\right\} + n_{(i-1)i} \end{aligned} \tag{24}$$

$$\begin{aligned} u_i(\tau,\eta) &= \omega_r\left\{\tau-\frac{2R_i(\eta)}{c}\right\}\omega_a\{\eta-\eta_c\} \\ &\quad\times\exp\left\{j\pi K_r\left(\tau-\frac{2R_i(\eta)}{c}\right)^2\right\}. \end{aligned} \tag{25}$$

Since $2R_{i-1}(\eta)/c \approx 2R_i(\eta)/c$, we can get the approximation: $u_{i-1}(\tau,\eta)\approx u_i(\tau,\eta)$, and then, $s_{(i-1)i}(\tau,\eta)$ can be reformulated as

$$\begin{aligned} s_{(i-1)i}(\tau,\eta) &= g_{(i-1)i}(\eta)\,u_i(\tau,\eta)\exp\left\{-j4\pi\frac{R_{i-1}(\eta)}{\lambda}\right\} \\ &\quad - u_i(\tau,\eta)\exp\left\{-j4\pi\frac{R_i(\eta)}{\lambda}\right\} + n_{(i-1)i} \\ &= v_i(\eta)\,u_i(\tau,\eta)\exp\left\{-j4\pi\frac{R_i(\eta)}{\lambda}\right\} + n_{(i-1)i} \\ &= v_i(\eta)\,s_{Ti}(\tau,\eta) + n_{(i-1)i} \end{aligned} \tag{26}$$

where $v_i(\eta)$ represents the azimuth modulation caused by the cancellation process, which is expressed as

$$v_i(\eta) = g_{(i-1)i}(\eta)\exp\left\{-j4\pi\frac{R_{i-1}(\eta)-R_i(\eta)}{\lambda}\right\} - 1. \tag{27}$$

Through the joint cancellation filter $\mathbf{G}(\eta)$, the two adjacent channels are canceled separately to eliminate the jamming signal and retain the useful target echo.

C. Signal Reconstruction

For the multichannel signals after the joint cancellation processing, their sampling frequency clearly cannot reach the Nyquist sampling frequency, which will result in azimuth ambiguity. To achieve unambiguous imaging, signal reconstruction needs to be conducted. It is worth noting that only the data of $I-1$ channels remained after channel cancellation processing, which means the equivalent PRF after signal reconstruction need to satisfy $(I-1)\text{PRF} \geq B_a$, where B_a is the Doppler bandwidth of the system. The reconstruction algorithm [33] comprises the following three steps.

1) An azimuth Fourier transform is performed to convert the signals in (23) to the range-Doppler domain as

$$\mathbf{S}_1(\tau, f_\eta) = \int \mathbf{s}_1(\tau, \eta) \exp\{-j2\pi f_\eta \eta\} d\eta \tag{28}$$

where $f_\eta \in [-\text{PRF}/2, \text{PRF}/2]$ signifies the Doppler frequency.

2) Let $N = I-1$, and the prefilter matrix is established as

$$\mathbf{H}(f_\eta) = \begin{bmatrix} h_{12}(f_{\eta,1}) & h_{12}(f_{\eta,2}) & \cdots & h_{12}(f_{\eta,N}) \\ h_{23}(f_{\eta,1}) & h_{23}(f_{\eta,2}) & \cdots & h_{23}(f_{\eta,N}) \\ \vdots & \vdots & \ddots & \vdots \\ h_{(I-1)I}(f_{\eta,1}) & h_{(I-1)I}(f_{\eta,2}) & \vdots & h_{(I-1)I}(f_{\eta,N}) \end{bmatrix} \tag{29}$$

with

$$h_{(i-1)i}(f_{\eta,n}) = \exp\left\{-j\pi f_{\eta,n} \frac{\Delta x_i}{V_r}\right\} \exp\left\{-j\pi \frac{\Delta x_i^2}{2\lambda R_0}\right\} \tag{30}$$

where $f_{\eta,n} = f_\eta + (n - \frac{N+1}{2})\text{PRF}, n = 1, 2, \ldots, N$, belongs to nth spectrum component.

Then, the reconstruction filter matrix $\mathbf{P}(f_\eta)$ is derived from an inversion of the matrix $\mathbf{H}(f_\eta)$ as

$$\mathbf{P}(f_\eta) = \mathbf{H}^{-1}(f_\eta). \tag{31}$$

3) Reconstruct $\mathbf{S}_1(\tau, f_\eta)$ using the matrix $\mathbf{P}(f_\eta)$ as

$$\mathbf{S}_2(\tau, f_\eta) = \mathbf{P}(f_\eta)\mathbf{S}_1(\tau, f_\eta). \tag{32}$$

After rearranging the spectrum of the reconstructed signal $\mathbf{S}_2(\tau, f_\eta)$, an equivalent single channel signal with sampling rate of $(I-1)\cdot \text{PRF}$ is obtained. And an HRWS image without jamming can be acquired by the imaging algorithm such as chirp-scaling algorithm (CSA).

D. Azimuth Compensation

According to (27), we can know that the azimuth modulation function generated by the joint cancellation processing is related to the location of the target and the jammer in the imaging area, so it can be rewritten as

$$v_i(\eta) = \exp\left\{-j\frac{2\pi}{\lambda}\Delta\varphi\right\} - 1 \tag{33}$$

with

$$\Delta\varphi = R_{Ji}(\eta) - R_{J(i-1)}(\eta) + R_{R(i-1)}(\eta) - R_{Ri}(\eta). \tag{34}$$

The Taylor series expansion, which is retained to the quadratic term, is performed to the distance term in (34), and after simplification, $v_i(\eta)$ can be rewritten as

$$v_i(\eta) = \exp\left\{-j\frac{2\pi}{\lambda}\Delta\varphi_1 + j\frac{2\pi}{\lambda}\Delta\varphi_2\right\} - 1 \tag{35}$$

with

$$\Delta\varphi_1 = \frac{[2V_r\eta - 2y_J - (2\cdot i_{\text{ref}} - 2i + 1)\,d]\,d}{2R_J} \tag{36}$$

$$\Delta\varphi_2 = \frac{[2V_r\eta - (2\cdot i_{\text{ref}} - 2i + 1)\,d]\,d}{2R_0}. \tag{37}$$

Since the jammer is usually located in the imaging area, the following approximation holds [34]: $R_J \approx R_0$, so there are

$$v_i(\eta) \approx \exp\left\{j\frac{2\pi}{\lambda}\frac{d\cdot y_J}{R_0}\right\} - 1. \tag{38}$$

According to (38), we can find that the azimuth modulation function at the target is only related to the azimuth position y_J of the jammer. For the whole imaging area, the azimuth modulation function can be expressed as

$$h(y) = \exp\left\{j\frac{2\pi}{\lambda}\frac{d\cdot(y - y_J)}{R_0}\right\} - 1 \tag{39}$$

where y is the azimuth position of the target in the imaging area. It can be seen that the modulation function $h(y)$ is periodic along the azimuth direction with an amplitude variation range of [−2,0] and a period of $\frac{\lambda R_0}{d}$, which result in the periodic dark stripes in the focused image along the azimuth direction. At $y_{J0} = k\cdot\frac{\lambda R_0}{d} + y_J, k = 0, \pm1, \pm2, \ldots$, which means $h(y) = 0$, the target echo is completely eliminated, and near y_{J0}, the amplitude of the target signal is severely weakened, so the image compensation is necessary. Since $h(y)$ is for the set of target points whose position is $(:, y, 0)$ along the azimuth, the image compensation is carried out point by point along the azimuth. In the echo domain, the echoes of target points located in a synthetic aperture time will be affected by each other, which cannot be distinguished. Therefore, the azimuth modulation caused by joint cancellation is compensated in the focused image domain.

The azimuth weighted compensation vector is constructed as

$$w(y) = \begin{cases} h(y)^{-1} & , h(y) \geq \beta \\ \beta^{-1} & , h(y) < \beta \end{cases} \tag{40}$$

where β is the threshold set according to the characteristics of the image, so as to avoid the situation that the denominator is close to 0 and affect the compensation effect.

Then, an HRWS SAR image after jamming suppression can be obtained by substituting (40) into the amplitude of the focused SAR image as

$$\mathbf{I} = \text{diag}\{w\}\,\mathbf{I}_e \tag{41}$$

where $\mathbf{I}_e$ is the imaging result of $\mathbf{S}_2(\tau, f_\eta)$.

TABLE I
SIMULATION SYSTEM PARAMETERS

Parameter	Symbol	Value
Nearest slant range	R_0	900 km
Carrier frequency	f_0	5.4 GHz
Signal pulse duration	T_r	20 μs
Signal bandwidth	B_r	110 MHz
Pulse repetition frequency	PRF	5457/1819 Hz
Doppler bandwidth	B_a	4962 Hz
Number of channels	I	4
Channel spacing	d	2.5 m
Platform velocity	V_r	7000 m/s

Hence, all of the processing steps have been completed and can be summarized as follows.

Step 1: Establish the least L^1-norm optimization model by (15) to locate the jammer.

Step 2: Suppress the jamming signal on the received contaminated multichannel signals using the joint cancellation filter (22), and the remaining echoes of $I-1$ channels without jamming are obtained.

Step 3: Reconstruct the jamming suppressed signals into a signal with a sampling rate of $(I-1)\cdot \mathrm{PRF}$ by (32) and focus it by CSA.

Step 4: Compensate the amplitude of the focused image along the azimuth direction by (41), and the uniform HRWS SAR image is obtained.

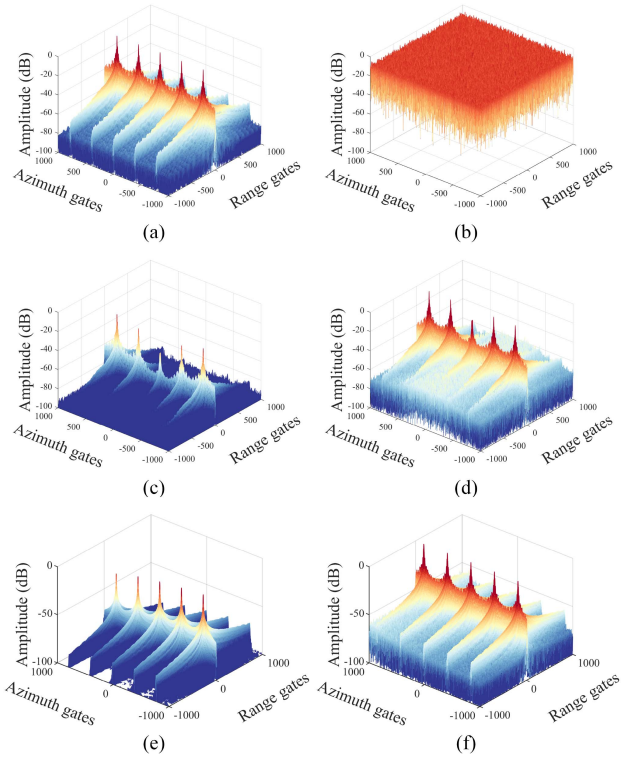

Fig. 3. Imaging result of the point target simulation. (a) Original image. (b) Jamming-corrupted image. (c) Result of dual-channel cancellation, PRF=5457 Hz. (d) Result of the proposed method, PRF=1819 Hz. (e) Result of dual-channel cancellation when the jammer is outside the imaging scene, PRF=5457 Hz. (f) Result of the proposed method when the jammer is outside the imaging scene, PRF=1819 Hz.

IV. SIMULATED AND REAL DATA PROCESSING RESULTS

In this section, some simulations and measured data experiment are carried out to evaluate the performance of the proposed JAMC scheme. The point target simulation is given in Section IV-A. Then, the scene simulation and the performance analysis are presented in Sections IV-B and IV-C, respectively. Finally, the measured airborne SAR data experiment is displayed in Section IV-D to verify the effectiveness of the proposed method.

A. Simulation of Point Target

The point targets simulation is performed to validate the proposed JAMC scheme. We simulated five point targets distributed along the azimuth direction with a 100-m distance separating. Table I lists the main simulation parameters of the multichannel SAR system. The original imaging result without jamming is shown in Fig. 3(a). For convenience, the center of the imaging scene is taken as the reference origin and the z-axis coordinate is omitted in the following discussion. The jammer is located in the center of the scene (0 m, 0 m) and coincides with the center point target p_3. Suppose the jamming signal emitted by the jammer is in the form of Gaussian noise and remains constant during each pulse duration. The signal-to-interference ratio (SIR) is set to -50 dB. The imaging result with jamming is shown in Fig. 3(b). It can be seen that the point targets are completely submerged in the noise, and the imaging quality is seriously affected. Firstly, according to the least L^1-norm optimization model, the location of jammer can be obtained. It is worth noting that in order to facilitate the comparison with the real coordinates, all azimuth positions are deblurred by selecting the closest value to the center of the scene. So the estimated jammer coordinate is $(42.15\,\mathrm{m}, 0.00\,\mathrm{m})$.

The recovered images are presented in Fig. 3(c)–(f). In order to compare and illustrate the change of the amplitude at each point, the images are normalized by the maximum amplitude of their original images without jamming. Fig. 3(c) shows the imaging result after jamming suppression by dual-channel cancellation when the system PRF is 5457 Hz. Obviously, the jamming signal in the scene has been eliminated, but the signal amplitude has also been seriously weakened. According to (38), the azimuth modulation brought by the channel cancellation to the targets can be obtained, and the weighted value along the azimuth coordinate is shown in Fig. 4. The normalized amplitude values of the point targets in Fig. 3(c) and their theoretical amplitudes shown in Fig. 4 are listed in Table II. Clearly, the theoretical analysis agrees well with the experimental measurements. Therefore, the amplitude of the weakened signal can be well compensated according to the amplitude compensation function in (40).

Fig. 3(d) shows the imaging result by the proposed method when the PRF is 1819 Hz. It can be seen that the amplitude of the target is well recovered, and the PRF of the system is $1/3$

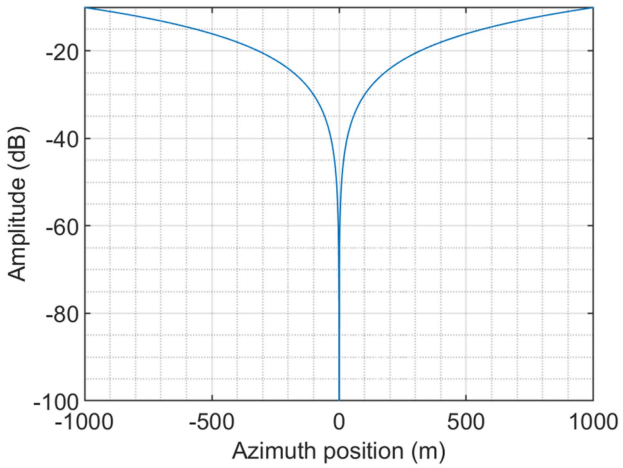

Fig. 4. Azimuth weighted value of Fig. 3(c) brought by the channel cancellation.

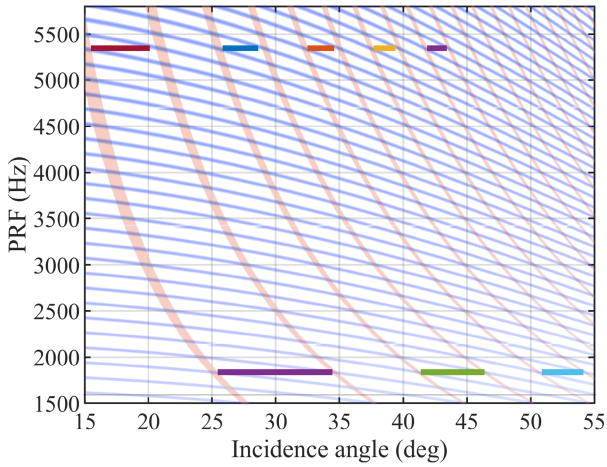

Fig. 6. Zebra map of the SAR system.

TABLE II
AMPLITUDES OF POINT TARGETS IN FIG. 3(C)

Amplitude(dB)	p_1	p_2	p_3	p_4	p_5
Theoretical	-23.99	-29.96	-	-30.16	-24.09
Measured	-24.02	-30.04	-48.41	-30.01	-24.03

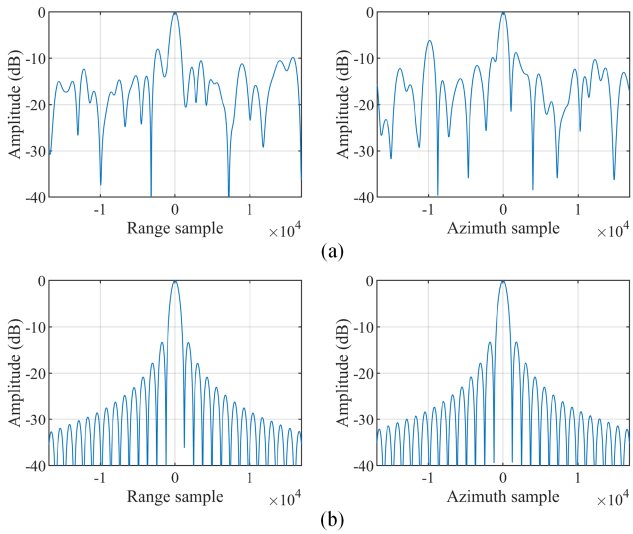

Fig. 5. IRFs in range and azimuth dimensions of p_1. (a) Range and azimuth profile of p_1 in Fig. 3(b). (b) Range and azimuth profile of p_1 in Fig. 3(d).

of that of the two-channel cancellation method. Fig. 5 shows the impulse response functions (IRFs) in range and azimuth dimensions of p_1 in Fig. 3(b) and (d). We can see that the jamming signal is completely removed and the point target is well recovered. Table III lists the peak-to-sidelobe ratio, integrated sidelobe ratio, and resolution measured in both range and azimuth dimensions. By comparing the metrics of the two tables, respectively, we can find that all the targets except p_3 in Fig. 3(d) can be restored to almost the same as that in Fig. 3(a). Analyzing the reason, since p_3 is in the same location as the jammer, it can be seen from (39) that the azimuth modulation value at this position is zero, so the signal of the target is theoretically eliminated, resulting in that the information of p_3 irrecoverable. In fact, only the targets that share the same azimuth position with the jammer is theoretically irrecoverable because of the azimuth modulation, whereas other point targets can all be well recovered. However, due to the receiver noise and the residual azimuth ambiguity, when the signal's amplitude is attenuated too much and below these noises, these signals will be submerged by the noise and cannot be restored.

When the jammer is outside the imaging scene, we set its coordinate to $(3000\,\mathrm{m}, 300.00\,\mathrm{m})$. The estimated position of the jammer by the least L^1-norm optimization model is $(3042.30\,\mathrm{m}, 299.99\,\mathrm{m})$. According to the estimated jammer position, the jamming suppression results by the two methods are presented in Fig. 3(e) and (f). Obviously, the dual-channel cancellation method requires a higher PRF, and the imaging result is also affected by the cancellation modulation. In contrast, the proposed JAMC algorithm can be used in low-PRF mode, and the imaging result can accurately restore the real scene. Hence, the proposed method is a great improvement over the dual-channel cancellation method.

For the PRF of the SAR system, it can be seen that the dual-channel cancellation method strictly requires the signals have unambiguous spectrum, so the PRF of the system is set to 5457 Hz, while the proposed method only needs 1819 Hz. Fig. 6 shows the zebra map of the SAR system. Obviously, the proposed method significantly increases the range of incident angles of the system, which means the HRWS imaging capability of the multichannel SAR system can be retained.

B. Simulation of Scene

In order to more intuitively show the performance of the proposed JAMC scheme, the simulation of scene is performed. The simulation still uses the parameters listed in Table I. Fig. 7 shows the simulation results. The original simulation image is shown in Fig. 7(a). The jammer is placed at the center of the scene $(0\,\mathrm{m}, 0\,\mathrm{m})$, and the SIR is set to -20 dB. The form

TABLE III
POINT-TARGET IMPULSE RESPONSE CHARACTERISTICS

	Imaging result without jamming in Fig.3(a) (Azimuth and range)						Processing results in Fig. 3(d) (Azimuth and range)					
Point Target	**Resolution (m)**		**PLSR (dB)**		**ILSR (dB)**		**Resolution (m)**		**PLSR (dB)**		**ILSR (dB)**	
1	1.25	1.21	-13.27	-13.32	-9.78	-9.91	1.24	1.21	-13.27	-13.37	-9.80	-9.92
2	1.25	1.21	-13.26	-13.25	-9.80	-9.90	1.25	1.21	-13.26	-13.33	-9.79	-9.91
3	1.25	1.21	-13.26	-13.25	-9.80	-9.89	3.57	2.77	-0.01	-0.02	0.72	1.68
4	1.25	1.21	-13.25	-13.23	-9.87	-9.86	1.25	1.21	-13.22	-13.29	-9.86	-9.86
5	1.25	1.21	-13.25	-13.23	-9.87	-9.86	1.25	1.21	-13.21	-13.28	-9.87	-9.86

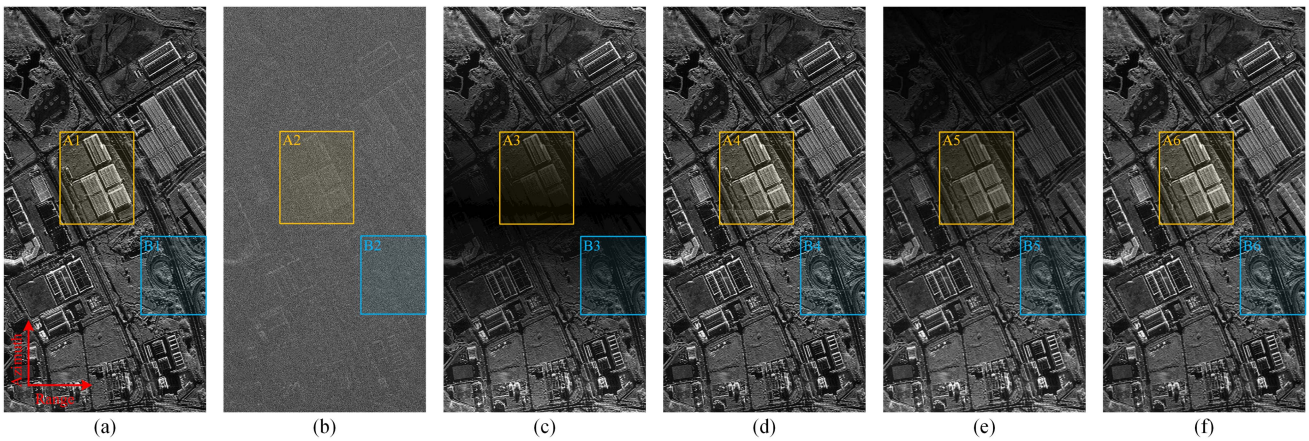

Fig. 7. Imaging results of simulated scene data. (a) Original image. (b) Jamming-corrupted image. (c) Result of dual-channel cancellation, PRF=5457 Hz. (d) Result of the proposed method, PRF=1819 Hz. (e) Result of dual-channel cancellation when the jammer is outside the imaging scene, PRF=5457 Hz. (f) Result of the proposed method when the jammer is outside the imaging scene, PRF=1819 Hz.

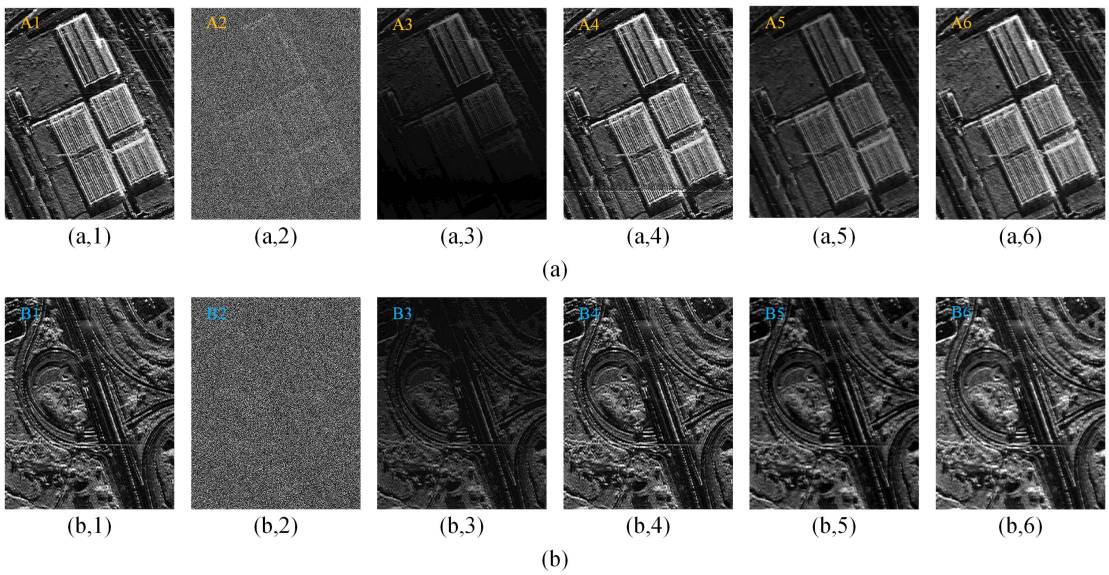

Fig. 8. Enlarged areas of yellow and blue rectangle in Fig. 7. (a) Factory area of yellow rectangle. (b) Overpass area of blue rectangle.

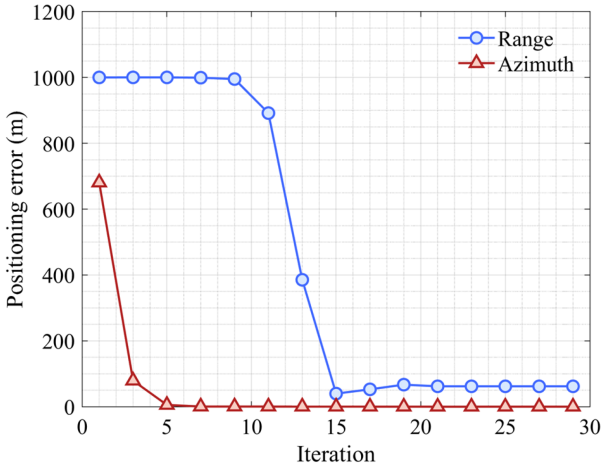

Fig. 9. Positioning error after each iteration.

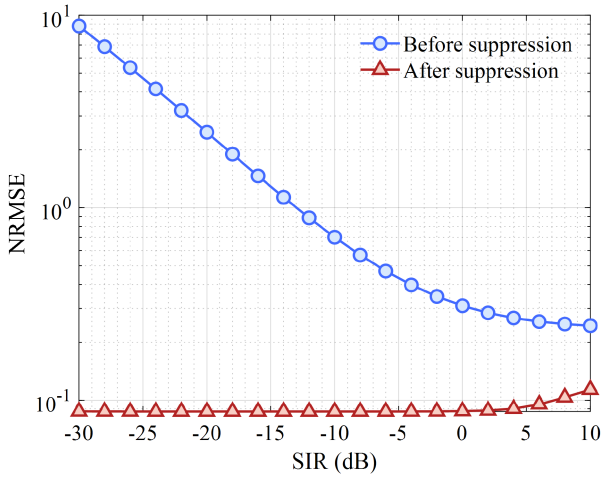

Fig. 12. Image NRMSE versus SIR.

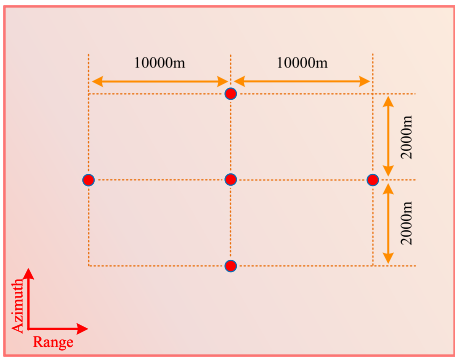

Fig. 10. Distribution of jammer.

TABLE IV
EXPERIMENTAL RESULTS

Jammer	Preset Location(m)	Estimated Result(m)	Absolute Error(m)
1	(0, 0)	(57.79, 0.00)	(57.79, 0.00)
2	(10000, 0)	(10056.94, 0.00)	(56.94, 0.00)
3	(-10000, 0)	(-9941.44, 0.00)	(58.56, 0.00)
4	(0, 2000)	(62.09, 1999.93)	(62.09, -0.07)
5	(0, -2000)	(62.32, -1999.93)	(62.32, 0.07)

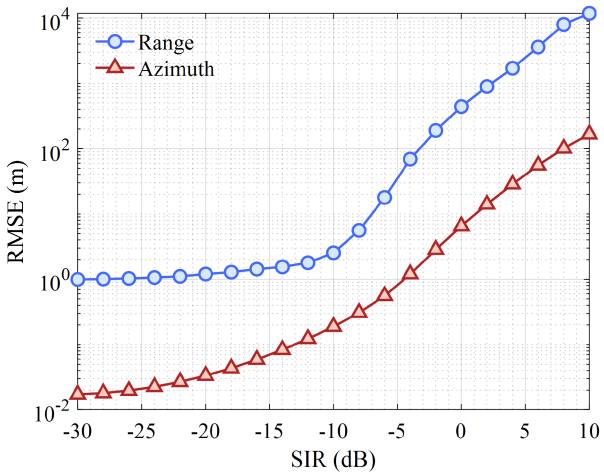

Fig. 11. Azimuth and range RMSEs versus SIR.

of the jamming signal is the same as that in Section IV-A. Fig. 7(b) presents the imaging results of the jamming-corrupted signals, as can be seen, the useful information is submerged in noise. First, the least L^1-norm optimization model is used to locate the jammer and the acquired coordinate of the jammer is $(57.79\,\mathrm{m}, 0.00\,\mathrm{m})$. Obviously, the localization result of the proposed algorithm is very close to the real coordinate of the jammer. Thus, the accuracy of the localization method is verified. Then, according to the estimated location of the jammer, we first use the dual-channel cancellation to suppress jamming when the PRF of system is 5457 Hz, and the result is illustrated in Fig. 7(c). It can be seen that the jamming signal is completely removed, but an azimuth modulation is brought to the image. Near the jammer, a dark strip is formed, which makes some targets unrecognizable and affects the readability of the image to some extent. Fig. 7(d) is the result of the joint cancellation method when the PRF of system is 1819 Hz. Clearly, the target information is basically restored, and the proposed method significantly reduces the high requirement of PRF.

Fig. 7(e) and (f) shows the results by the two methods when the jammer is outside the imaging scene. The coordinate of the jammer is set to $(5000\,\mathrm{m}, -1400\,\mathrm{m})$, and the estimated position is $(5062.31\,\mathrm{m}, -1399.93\,\mathrm{m})$. We can see that the imaging result can be accurately restored by the proposed method, while the result by dual-channel cancellation is seriously modulated.

In Fig. 8, we zoomed in the factory building and overpass areas of the images in Fig. 7, marked by A and B, respectively. From the factory building area in Fig. 8(a,4), it can be seen that several lines of targets near the azimuth location of the jammer are not well recovered. This is because the azimuth location of these targets are near the jammer. According to Fig. 4, we can know that the value of the azimuth modulation is very small, which causes the amplitude of these targets to be reduced too much, so that they are submerged by noises. However, at other areas that

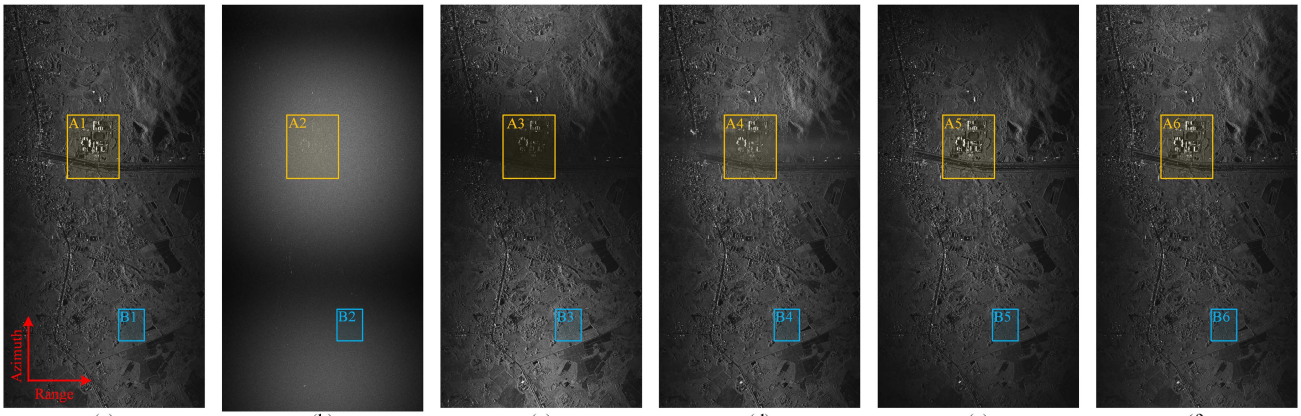

Fig. 13. Image recovery using the airborne SAR data. (a) Original SAR image scene. (b) Jamming-corrupted image. (c) Result of dual-channel cancellation, PRF=1293 Hz. (d) Result of the proposed method, PRF=431 Hz. (e) Result of dual-channel cancellation when the jammer is outside the imaging scene, PRF=1293 Hz. (f) Result of the proposed method when the jammer is outside the imaging scene, PRF=431 Hz.

not share the same azimuth coordinate with the jammer such as the overpass area shown in Fig. 8(b,4) and (b,6), the image processed by the proposed scheme can be recovered almost the same as the original image.

C. Analysis of Performance

The jammer localization method adopts the numerical solution method, while the other parts of the proposed JAMC scheme are simple matrix linear operations with low computational complexity, so we only measure the convergence speed of the localization method. The experiment uses the parameters in Table I and the SIR is set to -20 dB. The initial iterative value is $(0\,\mathrm{m}, 0\,\mathrm{m})$ and the jammer is placed at $(1000\,\mathrm{m}, 1000\,\mathrm{m})$. The iteration ends when the estimated location between two iterations is less than 10^{-2} m. Fig. 9 shows the positioning error after each iteration. It can be seen that the positioning error can almost reach the minimum after 15 iterations, as shown in Fig. 9. Furthermore, when we just need the jammer's azimuth location, a satisfying result can be got after only five iterations. It shows that the proposed jammer localization method can converge quickly.

In order to verify the robustness of the proposed jammer localization algorithm, localization experiments of jammers at different positions in the scene are carried out. The five jammers placed in sequence on the imaging scene are presented in Fig. 10. The SIR of them is still set to -20 dB and the jamming signal is in the form of Gaussian noise. The estimated location results are listed in the Table IV.

Obviously, the estimated position of the jammer is almost the same as the actual position, which means that the proposed method can achieve high-accuracy jammer location. It is worth noting that the proposed method is not affected by the position of the jammer in the scene, and the location estimation accuracy at the above five positions is at the same level. Another interesting phenomenon is that the azimuth position accuracy is significantly higher than the range direction. Usually, the nearest slant distance of spaceborne SAR is hundreds of kilometers, so the small change of the range position x_J has little effect on the phase compensation factor $g_{ij}(\eta, x_J, y_J)$. From (16), it is obvious that the change of the azimuth position y_J has a much greater influence on the result than the change of x_J, so the estimation accuracy of azimuth position will be higher than that of range position.

Since the proposed jammer localization method is based on the L^1-norm of the signal, the change of the SIR will also have an impact on the estimation result. The Monte Carlo experiments are carried out to verify the robustness of the proposed JAMC scheme according to the simulation of scene. The SIR varies from -30 to 10 dB with 1 dB steps. For each SIR, 50 Monte Carlo experiments are performed. The jammer's location is randomly set in each experiment, which has the uniform distribution on the interval of azimuth direction $(-1000\,\mathrm{m}, 1000\,\mathrm{m})$ and range direction $(-10\,000\,\mathrm{m}, 10\,000\,\mathrm{m})$ respectively. To evaluate the accuracy of the proposed localization method, the root-mean-square error (RMSE) is used with the following formulation:

$$\mathrm{RMSE} = \sqrt{\frac{1}{M}\sum_{m=1}^{M}(\hat{q}_m - q_m)^2} \tag{42}$$

where M is the number of experiments, and $\hat{q}_m$ and q_m are the estimated value and preset value in the mth experiment, respectively.

Fig. 11 presents the relationship between SIR and RMSE of the jammer's location. Obviously, when the SIR is greater than -5 dB, the estimation errors of the two begin to increase. This is because the channel cancellation will cause a certain loss to the real signal. When searching for the position of the jammer, if the variation of the jamming signal is smaller than that of the real signal, the positioning error will be caused, which is also the reason why the RMSE increases when the SIR is high. It can be seen that the proposed jammer localization method can obtain high accuracy when the SIR is below 0 dB.

Besides, in order to judge the performance of the proposed jamming suppression method, the normalized root-mean-square error (NRMSE) is used to evaluate the image quantitatively [35],

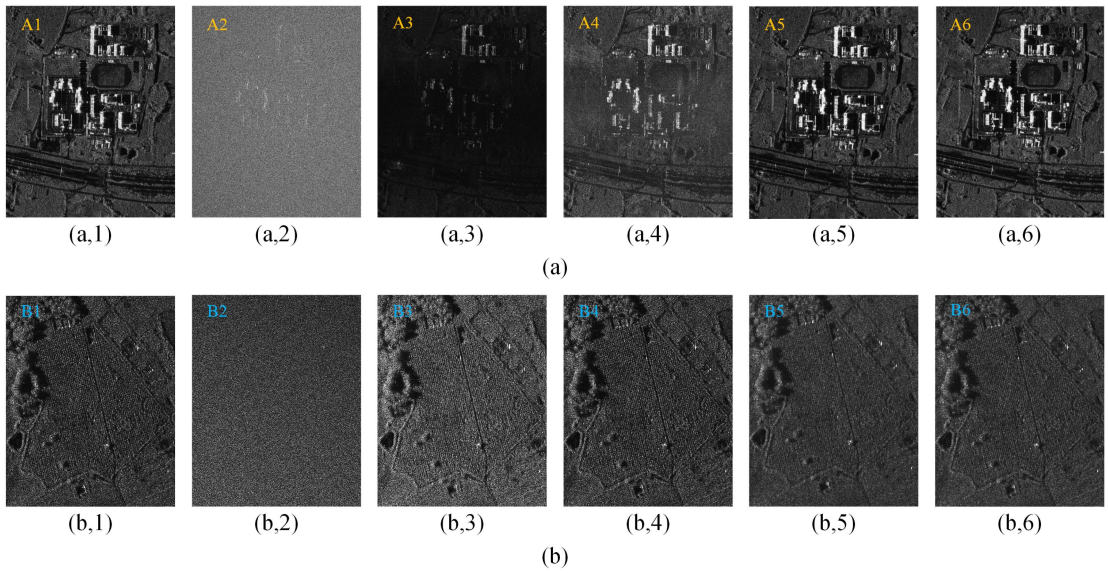

Fig. 14. Enlarged areas of yellow and blue rectangle in Fig. 13. (a) School area of yellow rectangle. (b) Farmland of blue rectangle.

i.e.,

$$\mathrm{NRMSE}(\mathbf{I}_0, \mathbf{I}) = \frac{\|\mathbf{I} - \mathbf{I}_0\|_F}{\|\mathbf{I}_0\|_F} \tag{43}$$

where $\mathbf{I}_0$ is the imaging result of original SAR echoes without jamming, and $\mathbf{I}$ is the imaging result of the recovered SAR signal. The smaller the NRMSE is, the better the performance of image restoration will be.

Fig. 12 illustrates the NRMSE of the contaminated images and final restored images. It can be seen that the NRMSE of the image before jamming suppression is large and decreases with the increase of SIR. In contrast, the NRMSE of the restored images are overall at a low level. This is because at low SIR, the estimated coordinate of the jammer is accurate, so the jamming signal is removed thoroughly and the image can be well restored. In the case of high SIR, the jamming energy itself is low and the impact on the image is limited, so the image can still be well recovered. Therefore, the value of NRMSE is relatively stable, which also verify the robustness of the proposed method.

D. Experiment of Airborne SAR Data

In this experiment, we demonstrate the effectiveness of the algorithm by analyzing the measured data. The data used were acquired by a *C*-band airborne multichannel SAR on September 27, 2014, which covered Hainan, China. The system works in the four-channel strip map mode and the main parameters are given in Table V. Suppose the jammer is placed in the school area of the scene and its coordinate is $(0\,\mathrm{m}, -800\,\mathrm{m})$. A high-power jamming signal in the form of Gaussian noise is constantly transmitted by the jammer and received by the four channels of the SAR.

Fig. 13(a) shows the original imaging area without jamming. Fig. 13(b) shows the imaging result of the contaminated echo with SIR of -20 dB. It can be seen that the imaging scene is covered by jamming and the target information is completely lost.

TABLE V
SIMULATION SYSTEM PARAMETERS

Parameter	Symbol	Value
Nearest slant range	R_0	14.4 km
Carrier frequency	f_0	5.4 GHz
Signal pulse duration	T_r	10.4 μs
Signal bandwidth	B_r	210 MHz
Pulse repetition frequency	PRF	1293/431 Hz
Doppler bandwidth	B_a	852 Hz
Number of channels	I	4
Channel spacing	d	0.156 m
Platform velocity	V_r	126.7 m/s

According to the proposed localization algorithm, the estimated location of the jammer is obtained and the coordinate is $(168.43\,\mathrm{m}, -799.30\,\mathrm{m})$, which is very close to the jammer's real location. Fig. 13(c) shows the imaging result after dual-channel cancellation when the PRF is 1293 Hz. The jamming signal is basically suppressed and the real targets can be displayed. However, the image amplitude fluctuates obviously along the azimuth direction due to the channel cancellation. The area marked by B3 is enhanced, whereas the area marked by A3 is weakened, and there is obvious dark stripe near the jammer, which affects the readability of the image to some extent. Fig. 13(d) shows the imaging result by the proposed method when the PRF is 431 Hz. It can be seen that the image is relatively uniform, and the system PRF is reduced by three times.

When the jammer is outside the imaging scene with the coordinate of $(5000\,\mathrm{m}, -2950\,\mathrm{m})$, we first obtain the estimated coordinate $(5173.14\,\mathrm{m}, -2950.71\,\mathrm{m})$, then the results by the above two methods are illustrated in Fig. 13(e) and (f). Clearly, the proposed method has a better performance.

Also, the enlarged areas marked by A and B, respectively, in Fig. 13 are shown in Fig. 14 with more details. It can be seen that in the school area near the jammer's azimuth location, the signal's amplitude after the channel cancellation is severely weakened, as is shown in Fig. 14(a,3). For the target with a small backscattering coefficient, the focused signal amplitude will be submerged by different noises. In this case, it is impossible to perform accurate amplitude compensation on the target signal, resulting in the loss of information for some weak targets in this area, such as the school area in Fig. 14(a,4). However, for the other areas which do not share the same azimuth coordinate with the jammer like the farmland shown in Fig. 14(b,4) and (b,6), they can all be well imaged without losing information. Therefore, the effectiveness of the proposed scheme is verified.

V. Conclusion

In this article, to locate the barrage jammer and suppress the jamming signals, a JAMC scheme is proposed for spaceborne SAR. First, the least L^1-norm optimization model of the signal is constructed in the echo domain, and the jammer coordinate in the scene can be estimated with high accuracy. Then, a joint cancellation filter is designed according to the phase difference of the jamming signal received by different channels of the SAR to remove the jamming signal. By reconstructing the remaining signal and the equivalent uniform sampling signal with unambiguous spectrum can be acquired. After imaging, the HRWS SAR image without jamming signal is preliminarily restored. Finally, for the periodic dark strips in the SAR image, the azimuth modulation function brought by the joint cancellation is deduced and compensated, and the uniform HRWS SAR image without jamming is obtained. The effectiveness of the proposed JAMC scheme is validated by both the simulation and real airborne SAR data experiments. In the future work, we will research the jamming suppression method in a multijammer environment.

References

[1] A. Moreira, P. Prats-Iraola, M. Younis, G. Krieger, I. Hajnsek, and K. P. Papathanassiou, "A tutorial on synthetic aperture radar," *IEEE Geosci. Remote Sens. Mag.*, vol. 1, no. 1, pp. 6–43, Mar. 2013.

[2] G. Krieger, N. Gebert, and A. Moreira, "Multidimensional waveform encoding: A new digital beamforming technique for synthetic aperture radar remote sensing," *IEEE Trans. Geosci. Remote Sens.*, vol. 46, no. 1, pp. 31–46, Jan. 2008.

[3] N. Li, Z. Lv, and Z. Guo, "Pulse RFI mitigation in synthetic aperture radar data via a three-step approach: Location, notch, and recovery," *IEEE Trans. Geosci. Remote Sens.*, vol. 60, 2022, Art. no. 5225617.

[4] M. Tao, F. Zhou, and Z. Zhang, "Wideband interference mitigation in high-resolution airborne synthetic aperture radar data," *IEEE Trans. Geosci. Remote Sens.*, vol. 54, no. 1, pp. 74–87, Jan. 2016.

[5] N. Li, Z. Lv, and Z. Guo, "Observation and mitigation of mutual RFI between SAR satellites: A case study between Chinese GaoFen-3 and European Sentinel-1A," *IEEE Trans. Geosci. Remote Sens.*, vol. 60, 2022, Art. no. 5112819.

[6] Y. Zhang et al., "First demonstration of echo separation for orthogonal waveform encoding MIMO-SAR based on airborne experiments," *IEEE Trans. Geosci. Remote Sens.*, vol. 60, 2022, Art. no. 5225016.

[7] Z. Li, H. Wang, T. Su, and Z. Bao, "Generation of wide-swath and high-resolution SAR images from multichannel small spaceborne SAR systems," *IEEE Geosci. Remote Sens. Lett.*, vol. 2, no. 1, pp. 82–86, Jan. 2005.

[8] W. Jing, M. Xing, C.-W. Qiu, Z. Bao, and T.-S. Yeo, "Unambiguous reconstruction and high-resolution imaging for multiple-channel SAR and airborne experiment results," *IEEE Geosci. Remote Sens. Lett.*, vol. 6, no. 1, pp. 102–106, Jan. 2009.

[9] I. Sikaneta, C. H. Gierull, and D. Cerutti-Maori, "Optimum signal processing for multichannel SAR: With application to high-resolution wide-swath imaging," *IEEE Trans. Geosci. Remote Sens.*, vol. 52, no. 10, pp. 6095–6109, Oct. 2014.

[10] C. Yang et al., "Pattern synthesis algorithm for range ambiguity suppression in the LT-1 mission via sequential convex optimizations," *IEEE Trans. Geosci. Remote Sens.*, vol. 60, 2021, Art. no. 2001713.

[11] Z. Chen et al., "A novel motion compensation scheme for 2-D multichannel SAR systems with quaternion posture calculation," *IEEE Trans. Geosci. Remote Sens.*, vol. 59, no. 11, pp. 9350–9360, Nov. 2021.

[12] S. Chang, Y. Deng, Y. Zhang, Q. Zhao, R. Wang, and K. Zhang, "An advanced scheme for range ambiguity suppression of spaceborne SAR based on blind source separation," *IEEE Trans. Geosci. Remote Sens.*, vol. 60, pp. 1–12, 2022.

[13] M. Bucciarelli, D. Cristallini, D. Pastina, M. Sedehi, and P. Lombardo, "Integrated wideband antenna nulling and focusing technique for multi-channel synthetic aperture radar," in *Proc. IEEE Int. Radar Symp.*, 2008, pp. 1–4.

[14] B. Zhao, F. Zhou, and Z. Bao, "Deception jamming for squint SAR based on multiple receivers," *IEEE J. Sel. Topics Appl. Earth Observ. Remote Sens.*, vol. 8, no. 8, pp. 3988–3998, Aug. 2015.

[15] W. Wang, J. Wu, J. Pei, Z. Sun, J. Yang, and Q. Yi, "Antirange-deception jamming from multijammer for multistatic SAR," *IEEE Trans. Geosci. Remote Sens.*, vol. 60, pp. 1–12, 2021.

[16] H. Hong-xu, Z. Yi-Yu, W. Jing, and H. Zhi-tao, "A frequency-based inter/intra partly coherent jamming style to SAR," in *Proc. IEEE 2nd Int. Conf. Signal Process. Syst.*, 2010, vol. 2, pp. V2–434.

[17] H.-x. Huang, Z.-t. Huang, and Y.-y. Zhou, "Jamming research to SAR based on frequency characteristic," in *Proc. IEEE 2nd Int. Conf. Signal Process. Syst.*, 2010, vol. 2, pp. V2–144.

[18] J. Yu et al., "Single RFI localization based on conjugate cross-correlation of dual-channel SAR signals," in *Proc. IEEE Int. Geosci. Remote Sens. Symp.*, 2019, pp. 385–388.

[19] X.-H. Lin, G.-Y. Xue, and P. Liu, "Novel data acquisition method for interference suppression in dual-channel SAR," *Prog. Electromagn. Res.*, vol. 144, pp. 79–92, 2014.

[20] L. Rosenberg and D. Gray, "Anti-jamming techniques for multichannel SAR imaging," *IEE Proc.-Radar, Sonar Navigat.*, vol. 153, no. 3, pp. 234–242, 2006.

[21] Y. Chunrui, Z. Yongsheng, Y. Anxi, D. Zhen, and L. Diannong, "Terrain scattered interference suppression for multichannel SAR," in *Proc. IEEE 3rd Int. Asia-Pacific Conf. Synthetic Aperture Radar (APSAR)*, 2011, pp. 1–4.

[22] D. Cerutti-Maori and I. Sikaneta, "A generalization of DPCA processing for multichannel SAR/GMTI radars," *IEEE Trans. Geosci. Remote Sens.*, vol. 51, no. 1, pp. 560–572, Jan. 2013.

[23] G. Rongbing, W. Jianguo, and H. Chuan, "Rebound jamming suppression by two-channel SAR," *Signal Process.*, vol. 21, no. 1, pp. 27–30, 2005.

[24] X.-y. Ma, J.-m. Qin, Z.-h. He, J. Yang, and Q.-H. Lu, "Three-channel cancellation of SAR blanketing jamming suppression," *ACTA Electonica Sinica*, vol. 35, no. 6, 2007, Art. no. 1015.

[25] Y. Junfei, L. Jingwen, S. Bing, and J. Yuming, "Barrage jamming detection and classification based on convolutional neural network for synthetic aperture radar," in *Proc. IEEE Int. Geosci. Remote Sens. Symp.*, 2018, pp. 4583–4586.

[26] H. Ruan, W. Ye, C. Yin, and S. Zhang, "Wide band noise interference suppression for SAR with dechirping and eigensubspace filtering," in *Proc. IEEE Int. Conf. Intell. Control Inf. Process.*, 2010, pp. 39–42.

[27] E. A. Yildirim and S. J. Wright, "Warm-start strategies in interior-point methods for linear programming," *SIAM J. Optim.*, vol. 12, no. 3, pp. 782–810, 2002.

[28] R. H. Byrd, J. C. Gilbert, and J. Nocedal, "A trust region method based on interior point techniques for nonlinear programming," *Math. Program.*, vol. 89, no. 1, pp. 149–185, 2000.

[29] J. Nocedal and S. J. Wright, *Numerical Optimization*. Berlin, Germany: Springer, 1999.

[30] Y. Cai, Y. Deng, H. Zhang, R. Wang, Y. Wu, and S. Cheng, "An image-domain least L1-norm method for channel error effect analysis and calibration of azimuth multi-channel SAR," *IEEE Trans. Geosci. Remote Sens.*, vol. 60, 2022, Art. no. 5222914.

[31] J. Feng, C. Gao, Y. Zhang, and R. Wang, "Phase mismatch calibration of the multichannel SAR based on azimuth cross correlation," *IEEE Geosci. Remote Sens. Lett.*, vol. 10, no. 4, pp. 903–907, Jul. 2013.
[32] H. Huang et al., "A novel channel errors calibration algorithm for multichannel high-resolution and wide-swath SAR imaging," *IEEE Trans. Geosci. Remote Sens.*, vol. 60, pp. 1–19, 2021.
[33] G. Krieger, N. Gebert, and A. Moreira, "Unambiguous SAR signal reconstruction from nonuniform displaced phase center sampling," *IEEE Geosci. Remote Sens. Lett.*, vol. 1, no. 4, pp. 260–264, Oct. 2004.
[34] X. Chang and C. Dong, "A barrage noise jamming method based on double jammers against three channel SAR GMTI," *IEEE Access*, vol. 7, pp. 18755–18763, 2019.
[35] Y. Huang, L. Zhang, J. Li, W. Hong, and A. Nehorai, "A novel tensor technique for simultaneous narrowband and wideband interference suppression on single-channel SAR system," *IEEE Trans. Geosci. Remote Sens.*, vol. 57, no. 12, pp. 9575–9588, Dec. 2019.

Shuohan Cheng received the B.S. degree in automation from Hunan University, Changsha, China, in 2019. She is currently working toward the Ph.D. degree with the Department of Space Microwave Remote Sensing System, Aerospace Information Research Institute, Chinese Academy of Sciences, Beijing, China.

She is also with the University of Chinese Academy of Sciences, Beijing. Her main research interests include synthetic aperture radar imaging and interference suppression.

Xilong Sun received the Ph.D. degree in signal processing from the National University of Defense Technology, Changsha, China, in 2012.

He is currently an Associate Researcher with the Beijing Remote Sensing Information Institute, Beijing, China. His research interests include synthetic aperture radar imaging and SAR jamming and antijamming.

Yonghua Cai was born in Chongqing, China, in 1996. He received the B.S. degree in communication engineering from Northwestern Polytechnical University, Xi'an, China, in 2019. He is currently working toward the Ph.D. degree with the National Key Laboratory of Microwave Imaging Technology, Aerospace Information Research Institute, Chinese Academy of Sciences, Beijing, China.

He is also with the University of Chinese Academy of Sciences, Beijing. His research interests include synthetic aperture radar imaging and signal processing.

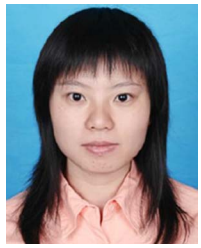

Huifang Zheng received the B.S. degree in electronic information engineering from Beijing Normal University, Beijing, China, in 2006, and the Ph.D. degree in communication and information systems from the University of Chinese Academy of Sciences, Beijing, in 2013.

She is currently working in the field of spaceborne synthetic aperture radar technology with the Aerospace Information Research Institute, Chinese Academy of Sciences.

Weidong Yu (Member, IEEE) received the M.Sc. and Ph.D. degrees in electrical engineering from the Nanjing University of Aeronautics and Astronautics, Nanjing, China, in 1994 and 1997, respectively.

Since 1997, he has been with the Institute of Electronics, Chinese Academy of Sciences (now the Aerospace Information Research Institute), Beijing, China. He has been the Professor and Chief Designer for several synthetic aperture radar (SAR) systems. His research interests include spaceborne SAR implementation and SAR signal processing.

Yanyan Zhang (Member, IEEE) received the B.S. degree in electronic and information engineering from Hunan University, Changsha, China, in 2017, and the Ph.D. degree in communication and information system from the University of Chinese Academy of Sciences, Beijing, China, in 2022.

His research interests include the system design and signal processing of bistatic/multistatic synthetic aperture radar (SAR), and high-resolution wide-swath SAR.

Sheng Chang received the B.S. degree in automation from Hunan University, Changsha, China, in 2019. He is currently working toward the Ph.D. degree in communication and information system with the University of Chinese Academy of Sciences, Beijing, China.

Since 2019, he has also been with the Department of Space Microwave Remote Sensing System, Aerospace Information Research Institute, Chinese Academy of Sciences, Beijing, where he has been involved in SAR systems design and signal processing. His main research interests include advanced spaceborne SAR concepts and signal processing.